PCCP

# Joint neutron/molecular dynamics vibrational spectroscopy reveals softening of HIV-1 protease upon binding of a tight inhibitor



| | |
|---|---|
| Journal: | *Physical Chemistry Chemical Physics* |
| Manuscript ID | CP-ART-12-2021-005487.R1 |
| Article Type: | Paper |
| Date Submitted by the Author: | 11-Jan-2022 |
| Complete List of Authors: | Kneller, Daniel; Oak Ridge National Laboratory<br>Gerlits, Oksana; Tennessee Wesleyan University<br>Daemen, Luke; Oak Ridge National Laboratory,<br>Pavlova, Anna; Georgia Institute of Technology College of Sciences<br>Gumbart, James; Georgia Institute of Technology College of Sciences,<br>Cheng, Yongqiang; Oak Ridge National Laboratory<br>Kovalevsky, Andrey ; Oak Ridge National Laboratory, Neutron Scattering Division |
| | |

# Joint neutron/molecular dynamics vibrational spectroscopy reveals softening of HIV-1 protease upon binding of a tight inhibitor

Daniel W. Kneller,[1] Oksana Gerlits,[2] Luke L. Daemen,[1] Anna Pavlova,[3] James C. Gumbart,[3] Yongqiang Cheng,[1] and Andrey Kovalevsky[1]*

[1]*Neutron Scattering Division, Oak Ridge National Laboratory, Oak Ridge, TN 37831, U.S.A.*

[2]*Department of Natural Sciences, Tennessee Wesleyan University, Athens, TN 37303, U.S.A.*

[3]*School of Physics, Georgia Institute of Technology, Atlanta, GA 30332, U.S.A.*

Corresponding author email: kovalevskyay@ornl.gov

## ABSTRACT

Biomacromolecules are inherently dynamic, and their dynamics are interwoven into function. The fast collective vibrational dynamics in proteins occurs in the low picosecond timescale corresponding to frequencies of ~5–50 $cm^{-1}$. This sub-to-low THz frequency regime covers the low-amplitude collective breathing motions of a whole protein and vibrations of the constituent secondary structure elements, such as α-helices, β-sheets and loops. We have used inelastic neutron scattering experiments in combination with molecular dynamics simulations to demonstrate the vibrational dynamics softening of HIV-1 protease, a target of HIV/AIDS antivirals, upon binding of a tight clinical inhibitor darunavir. Changes in the vibrational density of states of matching structural elements in the two monomers of the homodimeric protein are not identical, indicating asymmetric effect of darunavir on the vibrational dynamics. Three of the 11 major secondary structure elements contribute over 40% to the overall changes in the vibrational density of states upon darunavir binding. Molecular dynamics simulations informed by experiments allowed us to estimate that the altered vibrational dynamics of the protease would

contribute –3.6 kcal/mol at 300 K, or 25%, to the free energy of darunavir binding. As HIV-1 protease drug resistance remains a concern, our results open a new avenue to help establish a direct quantitative link between protein vibrational dynamics and drug resistance.

## INTRODUCTION

Dynamics is an inherent property of biomacromolecules written into the structure by the fundamental equation for the vibrational degrees of freedom, *3N–6* for a nonlinear molecule. Because macromolecules are comprised of thousands of atoms (*N*), they can have $10^4$-$10^5$ degrees of freedom (*e.g.*, for proteins containing ~200-2000 amino acid residues). The dynamical nature of biomacromolecules is essential for their biological activities such as cellular association, self-assembly, enzyme catalysis and to further reproductive fitness and self-organization.[1-5] The dynamic behavior of biomacromolecules spans at least fifteen orders of magnitude in time, occurring at timescales ranging from femtoseconds (fs or $10^{-15}$ s) to seconds in pursuit of environmental interactions to support life.[6] In protein molecules, atomic bond stretching and bending are among the fastest motions clocking in at 1-$10^2$ fs. Rotations and librations of amino acid residue side chains vary in frequency from tens of fs to tens of ps ($10^{-12}$ s) due to chemical diversity of amino acid sidechains and steric constrains in folded proteins. As the number of atoms participating in a particular motion increases, the amplitude also tends to increase, and the frequency tends to decrease. For instance, large conformational change events between distinct protein conformational states occur slowly (ns-μs or $10^{-9}$-$10^{-6}$ s) and infrequently and can be separated by large energy barriers (Figure 1).[7-11]

Collective vibrational dynamics within a protein molecule occur in a relatively discrete low-frequency regime from ~5–50 $cm^{-1}$ corresponding to the timescale of 0.66–6.7 ps.[12-14] Within this timescale protein breathing vibrational motions occupy the frequency ranges ~5–15 $cm^{-1}$ where dynamics are delocalized over the entire molecule. Collective motions of the protein secondary structure elements such as the accordion-like motions of α-helices, β-sheets and loops amass at the frequency range of ~15–50 $cm^{-1}$. Together, the breathing and secondary structure dynamics constitute the protein vibrational dynamics that determine protein stiffness or softness within this frequency regime. However, the protein dynamics at the fs–ps timescale are relatively unexplored.

Neutrons are ideal probes of biological matter and are well suited to study protein dynamics.[15,16] In particular, inelastic neutron scattering (INS) is the method of choice to probe the protein vibrational dynamics in the fs–ps time domain corresponding to the sub-to-low THz frequency regime. Cold neutrons have energies matching the protein vibrations, resulting in vibrational spectra with high neutron scattering amplitudes.[14,17-21] More importantly, INS spectra can reveal changes in the protein vibrational dynamics upon ligand binding.[22-28] This effect can be observed by comparing the intensity of inelastic scattering between the ligand-free and ligand-bound protein samples. An increase in neutron scattering intensity upon ligand binding, that is observing higher dynamic structure factors in the INS spectra, signifies softening of the protein vibrational dynamics, whereas reduction in intensity represents protein stiffening. Interestingly, it has been shown for several diverse proteins that substrate binding leads to the vibrational dynamics stiffening,[22,25-27] but inhibitor binding acts in the opposite direction resulting in the protein softening.[23]

HIV-1 protease (PR, Figure 2) is an important clinical drug target for treatment of HIV/AIDS.[29,30] PR is an aspartic protease enzyme that cleaves viral polyproteins to free the individual components required to produce infectious viral particles.[31] Two 99-residue PR chains organize to form a single active site cavity gated by two β-strand flaps within the catalytically active homodimer. An extensive structure-guided drug design campaign produced darunavir (DRV),[32] a clinical tight-binding competitive PR inhibitor with picomolar affinity for wild-type PR (Figure 2). Thorough understanding of the structural, electrostatic, and dynamic behavior of PR at traditional timescales makes the protein a platform well-suited to advance understanding of picosecond vibrational dynamics. The current study aims to characterize changes in the collective picosecond motions that result from DRV binding to wild-type PR. We used INS experiments of lyophilized $D_2O$-hydrated powders of hydrogenous PR to directly show that the vibrational dynamics of PR soften in the presence of DRV in the 5-60 $cm^{-1}$ frequency range. The INS spectra were reproduced with high fidelity using molecular dynamics (MD) simulations performed on the carefully constructed models with ten PR dimers representing the experimentally measured hydrated powder samples. By calculating the vibrational density of states (VDOS) from the MD simulations we demonstrated that altered vibrational dynamics are unequally distributed across the PR homodimer structure. Vibrational free energy calculations indicated that the vibrational dynamics contribute significantly, and favorably, to the free energy of DRV binding to PR.

## MATERIALS and METHODS

### Sample Preparation

HIV-1 PR was expressed and purified according to the previously described procedures.[33-35] Hydrogenated protein was dialyzed into a solution of 25 mM $NH_4OAc$, pH 5.5, at 4°C overnight. The final sample volume was split evenly into two parts. One aliquot received darunavir at a 2:1 molar ratio from a 40 mM stock made with DMSO, whereas the inhibitor-free protein sample received the identical volume of DMSO. After incubation on ice for 1 hour, samples were frozen at -80°C. Neutron scattering signal in the low-frequency regime stemming from hydrogens in ligand molecules in the sample is negligible compared to the signal from hydrogens in protein molecules.[27,36] Frozen samples were lyophilized (freeze-dried) for 3 days removing volatile $NH_4OAc$ to result in ~30-40 mg of dry samples. Under desiccated inert argon gas, the protein samples were transferred to aluminum weigh-boats (pouches) and then re-hydrated with 99.8% $D_2O$ vapor to ~40% w/w in a secondary closed box over 3 hours. Each sample was packaged into airtight 8 mm diameter vanadium sample holder cans for INS data collection.

### Inelastic neutron scattering measurements

INS measurements from the two HIV-1 PR samples were performed using the VISION neutron spectrometer at the Spallation Neutron Source of Oak Ridge National Laboratory. VISION is optimized for signal-to-noise ratios that measure molecular vibrations over a broad energy range of 0-8000 $cm^{-1}$ corresponding to the energy transfer of ~0-1000 meV at high resolutions by employing indirect-geometry spectrometry. Momentum transfer Q is a function of energy transfer, and the resolution of the VISION instrument is 1.5% of the energy transfer. Since VISION does not allow for Q resolution, VDOS cannot be directly calculated from experimental data. Q ranges from 1-4 $Å^{-1}$ for the energy range of interest for the protein sample under study.

Inhibitor-free and DRV-bound PR loaded vanadium sample holders, along with a sample holder containing an empty aluminum pouch, were cooled from room-temperature to 120 K and INS spectra were measured for ~24 hours each. Neutron scattering from the empty sample holder was subtracted from the protein INS spectra as background, and each spectrum was normalized to the elastic neutron scattering peak and the total measurement time by proton charge.

Protein samples were hydrated with $D_2O$ to minimize incoherent signal from the hydrogen in solvent. The contribution of coherent scattering of deuterium from the solvent is less than 5% of the total signal from the protium atoms in the protein molecules when using this preparation.[27] Combined with nearly equal hydration levels for both protein samples, coherent signal resulting from solvent is negligible and the dominant dynamic structure factors measured are from the incoherent neutron scattering from the hydrogen content of protein. Furthermore, incoherent scattering is the manifestation of the self-correlations of atoms in space and time and, therefore, structure factors are summed over all atoms. Thus, any observed differences in INS spectra between the two protein samples are assumed to arise from motions in the protein molecules, specifically altered vibrational motions.

Data collection was conducted at 120 K, below the glass-transition temperature of 180-200 K, to ensure atomic motions are harmonic and to simplify data interpretation by minimizing variables. Above the glass-transition temperature, anharmonic motions are introduced and overdamping of the low-energy modes of interest will contribute quasi-elastic scattering beyond the resolution range of VISION. [17,37-40] Direct experimental VDOS measurements from protein samples of trehalose-coated myoglobin below and above the glass-transition state temperature were found to be comparable.[41] Furthermore, vibrational modes from MD simulations performed at 300 K show that proteins are effectively harmonic at physiological temperatures.[42]

**Solution and powder molecular dynamics simulations**

Gromacs2020[43] was employed for all-atom classical molecular dynamics (MD) simulations to interpret the INS experiments. Crystal structures of HIV-1 protease in the closed conformation (PDB ID 4JEC with ligand removed),[44] semi-open conformation (PDB ID 1HHP),[45] wide-open conformation (PDB ID 1TW7),[46] and the DRV complex (PDB ID 2IEN)[47] in the closed conformation were used for solution MD simulations. NMR spectroscopy suggests wild-type inhibitor-free HIV-1 protease forms a population of flap conformations with distribution ratio of approximately 7:2:1 of closed:semi-open:open.[48] The powder model for MD simulations of inhibitor-free PR was populated accordingly, with ten PR dimers from starting representatives of each conformation.

PR dimers were described using the CHARMM36m[49] force field, whereas DRV was parameterized using CGenFF[50] then optimized with ffTK[51] as described below. Protonation states

were assigned in agreement with the room-temperature joint-X-ray/Neutron crystal structure PR in complex with amprenavir,[44] which is a close analogue of DRV. Each PR dimer was simulated using periodic boundary conditions in a rhombic dodecahedron box of water molecules (TIP3P)[52] with a minimum of 10 Å between any protein atom and the nearest cell edge. Chloride anions were used to neutralize the systems. Each system was then minimized to 5 $kJ \cdot mol^{-1}$ using the steepest descent algorithm before being equilibrated to 300 K using velocity rescaling[53] and 1 bar using the Berendsen barostat.[54] Production MD was performed for 1 μs for each inhibitor-free flap conformation and the DRV complex using the leapfrog integrator with a 2 fs integration step, Nose-Hoover[55,56] and Parrinello-Rahman[57] couplings, and bonds to hydrogen atoms constrained using the LINCS algorithm.[58,59] Long-range electrostatic interactions (beyond a 12-Å cutoff) were handled using the particle-mesh Ewald method.[60] Van der Waals interactions used the same cutoff with smoothing applied starting at 10 Å. Atom positions were saved every 10 ps. RMSD cluster analysis identified representative individual dimer structures used to populate a powder ensemble model. The top 10 snapshots from DRV-bound solution MD were used for the ligand-bound ensemble while the top 7 closed, 2 semi-open, and 1 open flap conformation representatives from the three individual inhibitor-free PR simulations were used to construct the inhibitor-free PR ensemble within the powder model.

Hydrated protein powder models have historically been used to simulate protein vibrations with protein atom and hydration water dynamics in good agreement with neutron spectroscopy data at a range of temperatures and hydration levels.[27,38,61-66] Conformationally variable amorphous hydrated protein powder models of inhibitor-free and DRV-bound enzyme were constructed by packing an ensemble of dimers solvated to experimental hydration levels (Figure 3). Protein molecules were inserted into a triclinic box with random rotations and translations one-by-one while extending the box along a single dimension. Water molecules were added in a shell around each molecule until experimental hydration was achieved and the system was neutralized using chloride anions. The powder system was minimized and equilibrated as performed for the single enzyme systems. Each system was cooled linearly from 300 K to 120 K over 1 ns. An unrestrained staging simulation was performed for 3 ns at 120 K prior to production MD. Production MD consisted of 40 ps simulations with a 1-fs integration step and a 1-fs coordinate collection rate. A minimum of 5 independent replicas of production MD were used for data analysis, including computation of VDOS and the INS spectra.

The well characterized nature of HIV-1 PR combined with recent advances in analysis software[67] enabled improvements from our previous methodology for aspartate amino transferase.[27] Specifically, we created substantially larger powder model systems of 10 protein dimers with embedded conformational variability consistent with known behavior of PR and performed a number of replica simulations. The internal protonation states were assigned with hydrogen positions accurately determined by neutron crystallography ensuring proper electrostatic distribution throughout the protein. Thus, we were able to sample the PR vibrational dynamics from a comparable timescale more confidently, enabling more sophisticated analyses to be performed.

**Force field parameterization of darunavir**

The structure of darunavir was uploaded to the CGenFF webserver, which assigns partial atomic charges and force field parameters to a molecule by analogy with the existing CGenFF parameters.[68,69] For each assignment a corresponding penalty score is also provided, and penalties higher than 10 indicate that validation of the assigned parameter may be needed. In the case of darunavir only two aliphatic carbons had partial atomic charge penalties of 11, whereas all other atoms had penalties lower than 10. Because aliphatic carbons do not form hydrogen bonds, and because the penalties were relatively low, we chose not to reoptimize any partial atomic charges. For the bonded terms, there were five dihedrals and one angle that needed to be re-optimized based on the penalties (Figure S1A). The Force Field Toolkit (ffTK) was used for optimization of the parameters and Gaussian16 (Gaussian 16, Revision B.01)[70] was used for quantum mechanical (QM) calculations at MP2/6-31G* level of theory, as recommended for CHARMM-compatible parameters.[50,51] Because the full darunavir molecule is too large for MP2 calculations, it was split into two parts referred to as Model 1 and Model 2 (Figures S1B and S1C). The geometries of the two structures were optimized, and relaxed dihedral scans in 15° increments were performed along the bonds with dihedrals that required optimization (Figure S1).[51] A Hessian calculation in internal coordinates was also performed for Model 2 and used for optimization of the angle parameter (Figure S1C). The force constant and the equilibrium value for the angle parameter were optimized to match the QM equilibrium value and QM energy for small angle displacements.[51] The dihedral parameters for both models were optimized to match the MM-generated dihedral scan energies to

the QM ones (Figures S1B and S1C).[51] The topology and parameters for DRV are included in the Supporting Information.

**Analysis of Experimental Model Molecular Dynamics**

The INS spectra and vibrational density of states (VDOS) were calculated from the trajectories of hydrated protein powder MD simulations using the OCLIMAX program[67,71] and processed further using in-house python scripts where necessary. The velocity autocorrelation function ($C_{(t)}$) was calculated using equation 1.1 for each atom to determine the statistical correlation of each atom over the timescale.

1.1 $$C_{(t)} = \left\langle \frac{\vec{v}_i(t + t_0) \cdot \vec{v}_i(t_0)}{\vec{v}_i \cdot \vec{v}_i(t_0)} \right\rangle$$

The VDOS power spectrum or phonon density of states ($g(\omega)$) (equation 1.2) is obtained by a Fourier transform of the velocity autocorrelation function $C_{(t)}$ and represents the quantity of vibrational modes as a function of energy frequency $\omega$. VDOS was normalized by integration of $g(\omega)$ to 1. When performing the discrete Fourier transformation, OCLIMAX employs the Hamming window function[72] (equation 1.3) to mitigate the spectral leakage due to truncation.

1.2 $$g(\omega) = \frac{1}{2\pi} \int \exp(-2i\pi\omega t) C_{(t)} dt$$

1.3 $$w(n) = 0.54 - 0.46\cos\left(\frac{2\pi n}{N}\right),\ 0 \le n \le N$$

From the normalized VDOS spectra, the fundamental excitation from coherent INS of each system can be computed by the incoherent inelastic neutron scattering function (equation 1.4) and compared to the experimental measurements. In equation 1.4, $q$ is the scattering vector, $\sigma_i$ and $m$ are the incoherent scattering cross section and mass of atom $i$, $W_d$ is the Debye-Waller factor, $n_s$ uses Planck's constant ($\hbar$) divided by Boltzmann's constant ($k_B$) times temperature (equation 1.5). For calculation of the INS contribution from solvent water atoms, the incoherent neutron scattering cross-section of deuterium was replaced with that of protium.

1.4 $$S_{inc\pm1}(q,\omega) = \sum_{i=1}^{N} \frac{\sigma_i}{6m_i} q^2 \exp(-2W_d) \frac{g(\omega)_i}{\omega} (n_s + \frac{1}{2} \pm \frac{1}{2})$$

1.5 $$n_s = \frac{1}{\exp\left(\frac{\hbar}{k_B T}\right) - 1}$$

Comparisons of VDOS between inhibitor-free and DRV-bound HIV-1 PR were performed. VDOS spectra calculated from the atom trajectories of each major secondary structure element of HIV-1 PR were compared for both systems to determine relative changes in low-frequency vibrational modes (1-60 $cm^{-1}$), where protein breathing motions and secondary structure vibrational dynamics occur, and their contribution to the changes in the vibrational dynamics of the whole protein. The partial integrated VDOS ($g_p$) for each secondary structure element was calculated using equation 1.6 in order to determine the relative changes in the number of vibrational modes for each element of each system (equation 1.7), where $a_1$:$a_2$ are the atoms range in that structural element and $\omega_1$-$\omega_2$ is the frequency range.

1.6 $$g_p = \frac{1}{\omega_2 - \omega_1} \int_{\omega_1}^{\omega_2} \frac{g(\omega) a_1{:}a_2}{a_2 - a_1} d\omega$$

1.7 $$relative\ change\ (\%) = \frac{[(g_p)element_{pr/drv} - (g_p)element_{pr}]}{[(g_p)element_{pr}]} \times 100$$

In order to evaluate how the relative changes in VDOS for each structural element contribute to the VDOS changes of the whole protein, the VDOS was calibrated to the degrees of freedom, $g_{cal}$ (equation 1.9), where $N$ is the number of atoms and $N_C$ is the number of hydrogen constraints. This can be done for each element for the frequency range of interest to calculate the overall contribution to change.

$$g_{cal} = (3N-6) - N_C = \gamma \int_{\omega_1}^{\omega_2} g(\omega) d\omega \text{ ;and thus } \gamma = \frac{(3N-6) - N_C}{\int_{\omega_1}^{\omega_2} g(\omega) d\omega}$$

1.8

$$contribution\ (\%) = \frac{\gamma element_{pr} - \gamma element_{pr/drv}}{\gamma protein_{pr/drv}} \times 100$$

1.9

Applying equation 1.10 affords calculation of the absolute VDOS ($g_{abs}$) and allows the vibrational partition function ($Z_{vib}$) associated with the vibrational energy levels in a harmonic system to be calculated as a function of frequency (equations 1.11 and 1.12).

1.10 $$g_{abs}\ (\omega) = \gamma_{abs} \cdot g(\omega), where\ \gamma_{abs} = \frac{(3N-6) - N_C}{\int_0^\infty g(\omega) d\omega}$$

1.11 $$Z_{vib} = \prod_{\omega\,=\,\omega_{min}}^{\infty} \left( \frac{e^{-\beta \hbar \omega/2}}{1 - e^{-\beta \hbar \omega}} \right)^{g_{abs}(\omega) d\omega}$$

1.12 $$\beta = \frac{1}{k_B T}$$

Finally, the Helmholtz vibrational free energy ($A_{vib}$) from protein atoms (equation 1.13) was computed from $Z_{vib}$ and was compared for the two systems.

1.13 $$A_{vib} = -\mathrm{RTln}(\mathrm{Z_{vib}}) = \sum_{\omega\,=\,\omega_{min}}^{\infty} g_{abs}(\omega)\ ln\left( \frac{e^{-\beta \hbar \omega/2}}{1 - e^{-\beta \hbar \omega}} \right)$$

## RESULTS and DISCUSSION

### INS reveals vibrational softening of PR when bound to DRV

Neutron vibrational spectroscopy was used to measure the vibrational modes of HIV-1 PR samples in the absence and presence of a tight-binding clinical inhibitor darunavir, DRV. The INS spectra of PR and PR/DRV samples are shown in Figures 4a and 4b. Amorphous materials, including proteins, produce a characteristic boson peak from ~ 5–150 $cm^{-1}$, where the signal results from low-frequency intraparticle vibrations and acoustic phonons stack.[40] The PR/DRV sample produces a more intense boson peak, thus higher dynamic structure factors, in the energy range of ~ 5–60 $cm^{-1}$ compared to inhibitor-free PR. The result indicates that PR possesses a greater amount

of vibrational amplitudes in the presence of DRV at the energy range corresponding to the collective vibrational behavior within the protein molecules at the low picosecond timescale of ~ 0.56–6.71 ps corresponding to 5–60 $cm^{-1}$. In this frequency range, breathing modes of the whole protein (5–15 $cm^{-1}$) and collective vibrations originating from the secondary structure vibrations (~15–50 $cm^{-1}$) occur. Beyond this range, higher-energy vibrational modes resulting from local side chain motions (~50–100 $cm^{-1}$) and bond rotations and translations (>100 $cm^{-1}$) are measured. Such localized motions of side chains are consistent between samples and are beyond the scope of this study which focuses on the picosecond vibrational dynamics of the whole enzyme and its constituent secondary structure elements. Thus, picosecond dynamics of the breathing modes and secondary structure elements in PR increase, leading to the vibrational softening of the protein when the enzyme interacts with DRV. The behavior of the PR vibrational dynamics is analogous to that previously observed for dihydrofolate reductase when it is bound to the clinical drug methotrexate.[23]

**MD simulations show DRV induces asymmetric changes in vibrational dynamics of PR dimer**

Powder MD simulations using models mimicking the samples measured in INS experiments were performed in order to interpret the low-frequency vibrational changes in PR that bring about the observed changes in the INS spectra for DRV-bound PR. Amorphous hydrated protein powder systems from 10 conformationally-variable dimers of either PR or PR/DRV were constructed to match INS experiments and compare the VDOS in the low-frequency energy regime (Figure 3). Atom velocities from 1 fs timesteps over 40 ps trajectories were used to compute the INS spectra. The boson peaks of the INS spectra from the simulated systems are in excellent agreement with experiment (Figure 4c) suggesting faithful recreation of an amorphous material in our MD simulations. Consistent with the INS experiments, the PR/DRV system exhibits significantly greater overall INS signal in the energy range of ~5–60 $cm^{-1}$ than inhibitor-free PR (Figures 4d and 4e) indicating softer vibrational dynamics for the inhibitor-bound enzyme.

The VDOS of PR atoms was extracted from the MD simulations to quantify the vibrational dynamics displayed by the protein. VDOS directly contributes to the INS signal and measures the magnitude of vibrational modes as a function of energy frequency. When the VDOS of the protein

atoms is examined across the low-frequency regime (Figure 5a), the relative difference displayed between the PR and PR/DRV systems follows an identical trend seen in the INS spectra of the hydrated systems as expected (Figure 5b). The result indicates that the vibrational modes displayed by PR are shifted to lower frequencies when the enzyme interacts with DRV. Induced fit of the enzyme to the ligand results from conformational shifts in the protein structure that might contribute to changes in picosecond vibrations and lead to the vibrational dynamics softening. As noted in the INS spectra (Figure 4d), the VDOS reveal a significant increase in the vibrational modes that correspond to the collective breathing vibrations of the whole protein molecule in the PR/DRV complex in the ~ 5–15 $cm^{-1}$ frequency range. This points to a significant softening of the PR breathing vibrations as well as secondary structure vibrations in the range of 15–60 $cm^{-1}$.

Each PR homodimer consists of distinct secondary structure elements that are coupled within the structure of each monomer. We considered these structural elements independently for each monomer for the purposes of deconvoluting the changes in the vibrational dynamics due to DRV binding and to find out whether these changes are asymmetric when the monomers are compared to each other. On the contrary, the intermolecular β-sheet at the N- and C-termini of PR dimer made up of four antiparallel β-strands and responsible for driving the PR dimerization was considered as one secondary structure element, because the four β-strands are tightly connected through a network of hydrogen bonds. It is of interest to identify the structural elements responsible for the significantly altered vibrations in the enzyme. VDOS was calculated using MD trajectories from the distinct structural elements as illustrated in Figure 6a. Each PR monomer is an identical chain of amino acid residues, but parsing structural elements independently yields more accurate information due to PR displaying asymmetric dynamics in the flexible flaps according to NMR data,[48,73] different protonation states of the central catalytic Asp25/Asp25′ residues, and the asymmetric chemical structure of DRV, although no obvious structural asymmetry between the monomers has been detected in PR crystal structures.[74,75] PR was primarily divided into secondary structure elements where the examined low-frequency vibrations are expected to originate as well as the active site residues and the intermolecular terminal β-sheet. The relative changes in VDOS as well as the contributions to the overall change from 1–60 $cm^{-1}$ for each structural element were calculated (Table 1) corresponding to collective vibrations of the secondary structure elements in the 0.56–33 ps time range. Overall contribution changes in VDOS are visualized for the PR dimer in Figure 6b. Relative partial VDOS provides information on the vibrational dynamics changes of

elements between systems. Moreover, the contribution to the overall VDOS change quantifies the extent of how each individual change in the vibrational dynamics of a secondary structural element contributes to the vibrational dynamics change of the entire protein molecule.

The changes in the individual structural element VDOS going from PR to PR/DRV are all positive except for β-sheet 2 in monomer B where vibrational dynamics stiffen in the DRV-bound state (Table 1 and Figure 7a-e). The greatest change in partial VDOS occurs in the flap of monomer A (Figure 7a) where PR closes on the aniline ring of DRV in the active site. Vibrational dynamics of the neighboring or distant elements can be coupled, which is observed for the flap and β-sheet 1 of monomer A where large relative changes (>5%) in VDOS occur (Figure 7b). Monomer A features only modest relative changes in VDOS (<3%) for the α-helix and β-sheet 2. In contrast, the largest changes in partial VDOS in monomer B were observed for the α-helix (Figure 7d) which is adjacent to β-sheet 2 where the only negative change occurred (Figure 7e). In the simulation, the aniline and *bis*-tetrahydrofuran groups of DRV interact with monomers A and B respectively and appear to contribute to asymmetric changes in the vibrational modes. Interestingly, the active sites of either monomer show minimal relative changes in VDOS (<1%) even though the corresponding amino acid residues have direct interactions with DRV. Structurally, the active site of PR consists of several loops which may have few collective motions at low frequencies. Relative changes in VDOS of PR are less pronounced than those calculated for either dihydrofolate reductase[36] or aspartate aminotransferase,[27] which could be due to the interplay of intrinsic structure-dynamics relationships in these enzymes. When the contributions of changes from secondary structure elements are considered in the context of the whole protein dimer, shifts in vibrational dynamics in just three structural elements in the PR dimer, specifically the flap and β-sheet 1 in monomer A and the α-helix in monomer B, contribute over 40% to the overall changes in VDOS after DRV binds to the protein (Table 1).

**Vibrational dynamics contributes to DRV binding energy**

Several factors contribute to the free energy of small molecule binding to protein that are either favorable such as formation of hydrogen bonds and hydrophobic interactions, and loss of hydration water, or unfavorable, including loss of translational and rotational degrees of freedom.[76,77] Moreover, as has been noted previously[23,78-82] the vibrational component associated with changes in the protein vibrational dynamics is not insignificant and can contribute at least

several kcal/mol to the free energy of binding. We therefore computed the Helmholtz vibrational free energy ($A_{vib}$) from the vibrational partition function ($Z_{vib}$), which is associated with the vibrational energy levels in a harmonic system, in order to assess the energetic consequences of the observed shifts in the PR vibrational dynamics upon DRV binding. The computed change in the vibrational free energy, $\Delta A_{vib}$, from the inhibitor-free to the DRV-bound system is –3.6 kcal/mol at 300 K, indicating favorable contribution of the vibrational dynamics to DRV binding. The total free energy of binding of DRV to the wild-type PR was previously measured by isothermal titration calorimetry to be –15.2 kcal/mol, which corresponds to the binding affinity of 4.5 pM.[83] Based on our calculations, we therefore estimate that the picosecond vibrational dynamics of PR contributes nearly 25% to the inhibitor binding energy, slightly less than that of methotrexate binding to dihydrofolate reductase (~40%)[23] where it was shown that the largest contributor to $\Delta A_{vib}$ was the increase in the protein vibrational entropy upon inhibitor binding. The protein-inhibitor complex accesses greater vibrational free energy than the inhibitor-free enzyme.

Our calculations demonstrate that the vibrational free energy landscape of a folded protein molecule is dominated by the collective motions of the secondary structure elements. Indeed, the $Z_{vib}$ spectra demonstrate that the vibrational energy for the protein originates from the low-frequency motions in the range of ~20-50 cm$^{-1}$ (Figure 8a). Plotting the ΔVDOS for protein atoms and $\Delta Z_{vib}$ as a function of frequency indicates where shifts in vibrational modes stemming from inhibitor binding result in significant changes in the vibrational free energy (Figure 8b). It is evident that, while significant changes in protein breathing modes (~ 5-15 cm$^{-1}$) occur, their effect on $Z_{vib}$ is negligible. Higher energy vibrational modes (> 50 cm$^{-1}$) also do not significantly contribute to $Z_{vib}$. Vibrational modes in the frequency range where secondary structure vibrational dynamics occur (~20-50 cm$^{-1}$) are the primary drivers of the $\Delta Z_{vib}$ for the PR/DRV complex and are the primary contributors to the free energy of DRV binding to PR.

## CONCLUSIONS

We have demonstrated that DRV binding to HIV-1 PR, an important drug target for the design and development of anti-HIV/AIDS antivirals, leads to the protein softening, with the increase in the picosecond vibrational dynamics arising from protein breathing and motions of the

secondary structure elements, such as helices and β-sheets. Vibrational dynamics changes of three structural elements, including the flap and β-sheet 1 in monomer A and the α-helix in monomer B, contribute over 40% to the overall changes in VDOS upon DRV binding. Importantly, the altered vibrational dynamics of PR upon DRV binding contributes ~ 25% to the favorable free energy of the inhibitor binding. HIV-1 evolves quickly to produce highly drug resistant variants of PR, such as PR20 with ~$10^4$ lower affinity to DRV than that of wild-type PR.[84] It is not unreasonable to suggest that changes in the picosecond vibrational dynamics due to mutations may be a novel unexplored mechanism of drug resistance. Hence, subsequent work will focus on discovering how drug resistant mutations alter PR vibrational dynamics and how these dynamical changes may translate into a considerable loss of inhibitor binding affinity to drug resistant PR variants.

## Author Information

D.W.K. and A.K. conceived and coordinated the study. O.G. carried out protein expression and purification. D.W.K. and A.K. prepared samples for neutron scattering. Y.C. and L.L.D. collected and processed inelastic neutron scattering data. J.C.G. and A.P. performed ligand parameterization and validation. D.W.K. and Y.C. carried out molecular dynamics simulations and performed computational analysis.

The manuscript was written through the contributions of all authors. All authors have given approval to the final version of the manuscript.

## Conflicts of interest

There are no conflicts to declare.

## Acknowledgements

Research at ORNL's Spallation Neutron Source (VISION beamline) was sponsored by the Scientific User Facilities Division, Office of Basic Energy Sciences, U.S. Department of Energy (DOE-BES). The Office of Biological and Environmental Research supported research at Oak

Ridge National Laboratory's Center for Structural Molecular Biology (CSMB) involving protein expression and purification, using facilities supported by the Scientific User Facilities Division, Office of Basic Energy Sciences, U.S. Department of Energy. Special thanks to Rhonda Moody of the User Labs and Sample Support at the Spallation Neutron Source for technical support during sample preparation for neutron scattering experiments. D.W.K is grateful to David Cashion of ORNL for excellent information technology support. D.W.K., Y.C., L.L.D. and A.K. were supported by the US Department of Energy's (DOE) Office of Basic Energy Sciences. J.C.G. acknowledges support from the National Institutes of Health (R01-AI148740) and computational resources through XSEDE (TG-MCB130173), which is supported by National Science Foundation grant ACI-1548562.

## REFERENCES

1. G.C.K. Roberts, Folding and unfolding for binding: large-scale protein dynamics in protein-protein interactions, *Biophys. Soc. Transact.*, 2006, **34**, 971-974.
2. K. Henzler-Wildman and D. Kern, Dynamic personalities of proteins, *Nature*, 2007, **450**, 964-972.
3. R. Matthews and C.N. Likos, Dynamics of self-assembly of model viral capsids in the presence of a fluctuating membrane, *J. Phys. Chem. B*, 2013, **117**, 8283-8292.
4. R. Callender, and R.B. Dyer, The dynamical nature of enzymatic catalysis. *Acc. Chem. Res.*, 2015, **48**, 407-413.
5. J.A. Byun, B. VanSchouwen, M. Akimoto and G. Melacini, Allosteric inhibition explained through conformational ensembles sampling distinct "mixed" states. *Comput. Struct. Biotech. J.*, 2020, **18**, 3803-3818.
6. K. Henzler-Wildman, M. Lei, V. Thai, S.J. Kerns, M. Karplus and D. Kern, A hierarchy of timescales in protein dynamics is linked to enzyme catalysis, *Nature*, 2007, **450**, 913-916.
7. M. Wolf-Watz, V. Thai, K. Henzler-Wildman, G. Hadjipavlou, E.Z. Eisenmesser, D. Kern, Linkage between dynamics and catalysis in a thermophilic-mesophilic enzyme pair, *Nat. Struct. Mol. Biol.*, 2004, **11**, 945.
8. Y.E. Shapiro, NMR spectroscopy on domain dynamics in biomacromolecules, *Prog. Biophys. Mol. Biol.*, 2013, **112**, 58-117.
9. S.S. Taylor, P. Zhang, J.M. Steichen, M.M. Keshwani and A.P. Kornev, PKA: lessons learned after twenty years, *Biochim. Biophys. Acta*, 2013, **1834**, 1271-1278.
10. A.K. Srivastava, L.R. McDonald, A. Cembran, J. Kim, L.R. Masterson, C.L. McClendon, S.S. Taylor and G. Veglia, Synchronous opening and closing motions are essential for cAMP-

dependent protein kinase A signaling, *Structure*, 2014, **22**, 1735-1743.

11. Y. Hao, J.P. England, L. Bellucci, E. Paci, H.C. Hodges, S.S. Taylor and R.A. Maillard, Activation of PKA via asymmetric allosteric coupling of structurally conserved cyclic nucleotide binding domains, *Nat. Commun.*, 2019, **10**, 3984.
12. B. Brooks and M. Karplus, Harmonic dynamics of proteins: normal modes and fluctuations in bovine pancreatic trypsin inhibitor, *Proc. Natl. Acad. Sci. U.S.A.*, 1983, **80**, 6571-6575.
13. K.-C. Chou, Low-frequency collective motion in biomacromolecules and its biological functions. *Biophys. Chem.*, 1988, **30**, 3-48.
14. S. Cusack, J. Smith, J. Finney, B. Tidor and M. Karplus, Inelastic neutron scattering analysis of picosecond internal protein dynamics. Comparison of harmonic theory with experiment. *J. Mol. Biol.*, 1988, **202**, 903-908.
15. M.M. Castellanos, A. McAuley and J.E. Curtis, Investigating structure and dynamics of proteins in amorphous phases using neutron scattering. *Comput. Struct. Biotechnol. J.*, 2017, **15**, 117-130.
16. G. Schiro, Probing the dynamics of biological matter by elastic, quasi-elastic, and inelastic neutron scattering, *EPJ Web Conf.*, 2020, **236**, 05001.
17. S. Cusack and W. Doster, Temperature dependence of the low frequency dynamics of myoglobin. *Biophys. J.*, 1990, **58**, 243-251.
18. A. Orecchini, A. Paciaroni, A.R. Bizzarri and S. Cannistraro, Low-frequency vibrational anolmalies in β-lactoglobulin: contribution of different hydrogen classes revealed by inelastic neutron scattering, *J. Phys. Chem. B*, 2001, **105**, 12150-12156.
19. J. Pieper, K.-D Irrgang, G. Renger and R.E. Lechner, Density of vibrational states of the light-harvesting complex II of green plants studied by inelastic neutron scattering, *J. Phys. Chem. B*, 2004, **108**, 10556-10565.
20. A.V. Frontzek, J.P. Embs, L. Paccou, Y. Guinet and A. Hedoux, Low-frequency dynamics of BSA complementarily studied by Raman and inelastic neutron spectroscopy, *J. Phys. Chem. B*, 2017, **121**, 5125-5132.
21. M. Yu, P. Tan, Y. Ye, D.J. Voneshen, X. Xing and L. Hong, One-dimensional nature of protein low-energy vibrations, *Phys. Rev. Res.*, 2020, **2**, 032050(R).
22. B. Jacrot, S. Cusack, A.J. Dianoux and D.M. Engelman, Inelastic neutron scattering analysis of hexakinase dynamics and its modification on binding of glucose, *Nature*, 1982, **300**, 84-86.
23. E. Balog, T. Becker, M. Oettl, R. Lechner, R. Daniel, J. Finney and J.C. Smith, Direct determination of vibrational density of states change on ligand binding to a protein, *Phys. Rev. Lett.,* 2004, **93**, 028103.
24. Y. Miao, Z. Yi, C. Cantrell, D.C. Glass, J. Baudry, N. Jain, and J.C. Smith, Coupled flexibility change in cytochrome P450cam substrate binding determined by neutron scattering, NMR, and molecular dynamics simulation, *Biophys. J.*, 2012, **103**, 2167-2176.
25. J. Peters, N. Martinez, M. Trovaslet, K. Scannapieco, M.M. Koza, P. Masson and F. Nachon,

Dynamics of human acetylcholinesterase bound to non-covalent and covalent inhibitors shedding light on changes to the water network structure, *Phys. Chem. Chem. Phys.*, 2016, **18**, 12992-13001.

26. K.A. Niessen, M. Xu, A. Paciaroni, A. Orecchini, E.H. Snell and A.G. Markelz, Moving in the right direction: protein vibrational steering function, *Biophys. J.*, 2017, **112**, 933-942.
27. S. Dajnowicz, Y. Cheng, L.L. Daemen, K.L. Weiss, O. Gerlits, T.C. Mueser and A. Kovalevsky, Substrate binding stiffens aspartate aminotransferase by altering the enzyme picosecond vibrational dynamics, *ACS Omega*, 2020, **5**, 18787-18797.
28. L.A.E.B. de Carvalho, A.P. Mamede, A.L.M.B. de Carvalho, J. Marques, G. Cinque, S. Rudic, and M.P.M. Marques, Metallodrug-protein interaction probed by synchrotron terahertz and neutron scattering spectroscopy. *Biophys. J.,* 2021, **120**, 3070-3078.
29. A. Engelman and P. Cherepanov, The structural biology of HIV-1: mechanistic and therapeutic insights, *Nat. Rev.*, 2012, **10**, 279-290.
30. A.K. Ghosh, H.L. Osswald and G. Prato, Recent Progress in the Development of HIV-1 Protease Inhibitors for the Treatment of HIV/AIDS, *J. Med. Chem.,* 2016, **59**, 5172-5208.
31. Z.Q. Beck, G.M. Morris and J.H. Elder, Defining HIV-1 Protease Substrate Selectivity, *Curr. Drug Targets,* 2002, **2**, 37-50.
32. S. De Meyer, H. Azijin, D. Surleraux, D. Jochmans, A. Tahri, R. Pauwels, P. Wigerinck and M.-P. de Bethune, TMC114, a novel human immunodeficiency virus type 1 protease inhibitor active against protease inhibitor-resistant viruses, including a broad range of clinical isolates. *Antimicrob. Agents Chemother.*, 2005, **49**, 2314–2321.
33. E.M. Wondrak and J.M. Louis, Influence of flanking sequences on the dimer stability of human immunodeficiency virus type 1 protease, *Biochemistry*, 1996, **35**, 12957–12962.
34. J.M. Louis, G.M. Clore and A.M. Gronenborn, Autoprocessing of HIV-1 protease is tightly coupled to protein folding, *Nat. Struct. Biol.*, 1999, **6**, 868–875.
35. B. Mahalingam, J.M. Louis, J. Hung, R.W. Harrison and I.T. Weber, Structural implications of drug-resistant mutants of HIV-1 protease: high-resolution crystal structures of the mutant protease/substrate analogue complexes, *Proteins Struct. Funct. Bioinforma.*, 2001, **43**, 455–464.
36. E. Balog, D. Perahia, J.C. Smith and F. Merzel, Vibrational softening of a protein on ligand binding, *J. Phys. Chem. B*, 2011, **115**, 6811–6817.
37. W. Doster, S. Cusack and W. Petry, Dynamical transition of myoglobin revealed by inelastic neutron scattering, *Nature*, 1989, **337**, 754-756.
38. Y. Joti, H. Nakagawa, M. Kataoka and A. Kitao, Hydration effect on low-frequency protein dynamics observed in simulated neutron scattering spectra, *Biophys. J.,* 2008, **94**, 4435-4443.
39. A.M. Tsai, D.A. Neumann and L.N. Bell, Molecular dynamics of solid-state lysozyme as affected by glycerol and water: a neutron scattering study, *Biophys. J.*, 2000, **79**, 2728–2732.
40. V. Kurkal-Siebert and J.C. Smith, Low-temperature protein dynamics: a simulation analysis

of interprotein vibrations and the Boson peak at 150 K, *J. Am. Chem. Soc.*, 2006, **128**, 2356-2364.

41. L. Cordone, M. Ferrand, E. Vitrano and G. Zaccai, Harmonic behavior of trehalose-coated carbon-monoxy-myoglobin at high temperature, *Biophys. J.*, 1999, **76**, 1043–1047.

42. A. Kitao, S. Hayward and N. Go, Energy landscape of a native protein: jumping-among-minima model, *Proteins*, 1998, **33**, 496–517.

43. M.J. Abraham, T. Murtola, R. Schulz, S. Páll, J.C. Smith, B. Hess and E. Lindahl, *SoftwareX*, 2015, **1**–**2**, 19–25.

44. I.T. Weber, M.J. Waltman, M. Mustyakimov, M.P. Blakeley, D.A. Keen, A.K. Ghosh, P. Langan and A.Y. Kovalevsky, Joint X-ray/Neutron crystallographic study of HIV-1 protease with clinical inhibitor amprenavir – insights for drug design, *J. Med. Chem.*, 2013, **56**, 5631–5635.

45. S. Spinelli, Q.Z. Liu, P.M. Alzari, P.H. Hirel and R.J. Poljak, The three-dimensional structure of the aspartyl protease from HIV-1 isolate BRU, *Biochimie*, 1991, **73**, 1391–1396.

46. P. Martin, J.F. Vickrey, G. Proteasa, Y.L. Jimenez, Z. Wawrzak, M.A. Winters, T.C. Merigan and L.C. Kovari, Wide open 1.3Å structure of a multi-drug resistant HIV-1 protease represents a novel drug target, *Structure*, 2005, **13**, 1887–95.

47. Y. Koh, S. Matsumi, D. Das, M. Amano, D. A. Davis, J. Li, S. Leschenko, A. Baldridge, T. Shioda, R. Yarchoan, A. K. Ghosh and H. Mitsuya, Potent inhibition of HIV-1 replication by novel non-peptidyl small molecule inhibitors of protease dimerization, *J. Biol. Chem.*, 2007, **282**, 28709–28720.

48. J. Roche, J.M. Louis and A. Bax, Conformation of inhibitor-free HIV-1 protease derived from NMR spectroscopy in a weakly oriented solution, *Chembiochem*, 2015, **16**, 214–218.

49. J. Huang, S. Rauscher, G. Nawrocki, T. Ran, M. Feig, B.L. De Groot, H. Grubmüller and A.D. MacKerell, CHARMM36m: an improved force field for folded and intrinsically disordered proteins, *Nat. Methods*, 2017, **14**, 71–73.

50. K. Vanommeslaeghe, E. Hatcher, C. Acharya, S. Kundu, S. Zhong, J. Shim, E. Darian, O. Guvench, P. Lopes, I. Vorobyov and A.D. Mackerell, CHARMM general force field: a force field for drug-like molecules compatible with the CHARMM all-atom additive biological force fields, *J. Comput. Chem.*, 2010, **31**, 671–690.

51. C.G. Mayne, J. Saam, K. Schulten, E. Tajkhorshid and J.C. Gumbart, Rapid parameterization of small molecules using the Force Field Toolkit, *J. Comput. Chem.*, 2013, **34**, 2757–2770.

52. W.L. Jorgensen, J. Chandrasekhar, J.D. Madura, R.W. Impey and M.L. Klein, Comparison of simple potential functions for simulating liquid water, *J. Chem. Phys.*, 1983, **79**, 926–935.

53. G. Bussi, D. Donadio and M. Parrinello, Canonical sampling through velocity rescaling, *J. Chem. Phys.*, 2007, **126**, 014101.

54. H.J.C. Berendsen, J.P.M. Postma, W.F. Van Gunsteren, A. Dinola and J.R. Haak, Molecular dyanmics with coupling to an external bath, *J. Chem. Phys.*, 1984, **81**, 3684–3690.

55. S. Nosé, A molecular dyanmics method for simulations in the canonical ensemble, *Mol. Phys.*, 1984, **52**, 255–268.

56. W.G. Hoover, Canonical dynamics: equilibrium phase-space disctributions, *Phys. Rev. A*, 1985, **31**, 1695–1697.

57. M. Parrinello and A. Rahman, Polymorphic transitions in single crystals: a new molecular dynamics method, *J. Appl. Phys.*, 1981, **52**, 7182–7190.

58. B. Hess, H. Bekker, H.J.C. Berendsen and J.G.E.M. Fraaije, LINCS: a linear constraint solver for molecular simulations, *J. Comput. Chem.*, 1997, **18**, 1463–1472.

59. B. Hess, P-LINCS: a parallel linear constraint solver for molecular simulations, *J. Chem. Theory Comput.*, 2008, **4**, 116–122.

60. T. Darden, D. York and L. Pedersen, Particle mesh Ewald: an $N\cdot\log(N)$ method for Ewald sums in large systems, *J. Chem. Phys.*, 1993, **98**, 10089–10092.

61. K. Wood, A. Frölich, A. Paciaroni, M. Moulin, M. Härtlein, G. Zaccai, D. J. Tobias and M. Weik, Coincidence of dynamical transitions in a soluble protein and its hydration water: direct measurements by neutron scattering and MD simulations, *J. Am. Chem. Soc.*, 2008, **130**, 4586–4587.

62. M. Tarek and D.J. Tobias, Environmental dependence of the dynamics of protein hydration water, *J. Am. Chem. Soc.*, 1999, **121**, 9740–9741.

63. M. Tarek and D.J. Tobias, The dynamics of protein hydration water:a quatitative comparison of molecular dynamics simulations and incoherent neutron scattering experiments, *Biophys. J.*, 2000, **79**, 3244–3257.

64. M. Tarek, G.J. Martyna and D.J. Tobias, Amplitudes and frequences of protein dynamics: an analysis of discrepancies between neutron scattering and molecular dynamics simulations, *J. Am. Chem. Soc.*, 2000, **122**, 10450–10451.

65. H. Nakagawa and M. Kataoka, How can we derive hydration water dynamics with inceherent neutron scattering and molecular dynamics simulation? *Biophys. Physicobiology*, 2019, **16**, 213-219.

66. D. Vural, Dynamics of lignin: molecular dynamics and neutron scattering, *ACS Symposium Series*, American Chemical Society, 2019, *1338*, pp. 49–67.

67. Y.Q. Cheng, L.L. Daemen, A.I. Kolesnikov and A.J. Ramirez-Cuesta, Simulation of inelastic neutron scattering spectra using OCLIMAX, *J. Chem. Theory Comput.*, 2019, **15**, 1974–1982.

68. K. Vanommeslaeghe and A.D. MacKerell, Jr., Automation of the CHARMM general force field (CGenFF) I: bond perception and atom typing, *J. Chem. Inf. Model.*, 2012a, **52**, 3144-3154.

69. K. Vanommeslaeghe, E.P. Raman and A.D. MacKerell, Jr., Automation of the CHARMM general force field (CGenFF) II: assignment of bonded parameters and partial atomic charges, *J. Chem. Inf. Model.*, 2012b, **52**, 3155-3168.

70. Gaussian 16, Revision B.01, M. J. Frisch, G. W. Trucks, H. B. Schlegel, G. E. Scuseria, M. A. Robb, J. R. Cheeseman, G. Scalmani, V. Barone, G. A. Petersson, H. Nakatsuji, X. Li, M. Caricato, A. V. Marenich, J. Bloino, B. G. Janesko, R. Gomperts, B. Mennucci, H. P. Hratchian, J. V. Ortiz, A. F. Izmaylov, J. L. Sonnenberg, D. Williams-Young, F. Ding, F. Lipparini, F. Egidi, J. Goings, B. Peng, A. Petrone, T. Henderson, D. Ranasinghe, V. G. Zakrzewski, J. Gao, N. Rega, G. Zheng, W. Liang, M. Hada, M. Ehara, K. Toyota, R. Fukuda, J. Hasegawa, M. Ishida, T. Nakajima, Y. Honda, O. Kitao, H. Nakai, T. Vreven, K. Throssell, J. A. Montgomery, Jr., J. E. Peralta, F. Ogliaro, M. J. Bearpark, J. J. Heyd, E. N. Brothers, K. N. Kudin, V. N. Staroverov, T. A. Keith, R. Kobayashi, J. Normand, K. Raghavachari, A. P. Rendell, J. C. Burant, S. S. Iyengar, J. Tomasi, M. Cossi, J. M. Millam, M. Klene, C. Adamo, R. Cammi, J. W. Ochterski, R. L. Martin, K. Morokuma, O. Farkas, J. B. Foresman, and D. J. Fox, Gaussian, Inc., Wallingford CT, 2016.

71. Y.Q. Cheng, A.I. Kolesnikov and A.J. Ramirez-Cuesta, Simulation of inelastic neutron scattering spectra directly from molecular dynamics trajectories, *J. Chem. Theory Comput.*, 2020, **16**, 7702–7708.

72. F.J. Harris, On the use of windows for harmonic analysis with the discrete Fourier transform, *Proc. IEEE*, 1978, **66**, 51–83.

73. V.Yu. Torbeev, H. Raghuraman, D. Hamelberg, M. Tonelli, W.M. Westler, E. Perozo and S.B.H. Kent, Protein Conformational Dynamics in the Mechanism of HIV-1 Protease Catalysis, *Proc. Natl. Acad. Sci. U.S.A.,* 2011, **108**, 20982-20987.

74. O. Gerlits, T. Wymore, A. Das, C.-H. Shen, J.M. Parks, J.C. Smith, K. Weiss, D.A. Keen, M.P. Blakeley, J.M. Louis, P. Langan, I. Weber and A. Kovalevsky, Long-range electrostatics-induced two-proton transfer captured by neutron crystallography in an enzyme catalytic site, *Angew. Chem. Int. Ed.*, 2016, **55**, 4924-4927.

75. O. Gerlits, D.A. Keen, M.P. Blakeley, J.M. Louis, I.T. Weber and A. Kovalevsky, Room temperature neutron crystallography of drug resistant HIV-1 protease uncovers limitations of X-ray structural analysis at 100K, *J. Med. Chem.*, 2017, **60**, 2018-2025.

76. G.H. Peters, T.M. Frimurer, J.N. Andersen, O.H. Olsen, Molecular dynamics simulations of protein-tyrosine phosphatase 1B. II. Substrate-enzyme interactions and dynamics, *Biophys. J.*, 2000, **78**, 2191-2200.

77. X. Du, Y. Li, Y.-L. Xia, S.-M. Ai, J. Liang, P. Sang, X.-L. Ji and S.-Q. Liu, Insights into protein-ligand interactions: mechanisms, models, and methods, *Int. J. Mol. Sci.*, 2016, **17**, 144.

78. L. Zidek, M.V. Novotny, M.J. Stone, Increased protein backbone conformational entropy upon hydrophobic ligand binding, *Nat. Struct. Biol.*, 1999, **6**, 1118-1121.

79. S. Fischer, J.C. Smith and C.S. Verma, Dissecting the vibrational entropy change on protein/ligand binding: burial of a water molecule in bovine pancreatic trypsin inhibitor, *J. Phys. Chem. B*, 2001, **105**, 8050-8055.

80. D.M. Leitner, Energy flow in proteins. *Annu. Rev. Phys. Chem.*, 2008, **59**, 233-259.

81. V.R. Moorman, K.G. Valentine and A.J. Wand, The dynamical response of hen egg white

lysozyme to the binding of a carbohydrate ligand, *Prot. Sci.*, 2012, **21**, 1066-1073.

82. H. Gohlke, I.Y. Ben-Shalom, H. Kopitz, S. Pfeiffer-Marek and K.-H. Baringhaus, Rigidity theory-based approximation of vibrational entropy changes upon binding to biomolecules, *J. Chem. Theory Comput.*, 2017, **13**, 1495-1502.
83. N.M. King, M. Prabu-Jeyabalan, E.A. Nalivaika, P. Wigerinck, M.-P. de Bethune, C.A. Schiffer, Structural and thermodynamic basis for binding of TMC114, a next-generation human immunodeficiency virus type 1 protease inhibitor, *J. Virol.*, 2004, **78**, 12012-12021.
84. J. Agniswamy, C.-H. Shen, Y.-F. Wang, A.K. Ghosh, K.V. Rao, C.-X. Xu, J.M. Sayer, J.M. Louis and I.T. Weber, Extreme multidrug resistant HIV-1 protease with 20 mutations is resistant novel protease inhibitors with P1'-pyrrolidinone or P2-tris-tetrahydrofuran, *J. Med. Chem.*, 2013, **56**, 4017-4027.

**Table 1. Changes in low-frequency vibrational density of states for structural elements in HIV-1 PR after complexation with Darunavir**

Relative ΔVDOS and overall contribution integrated from 1-60 $cm^{-1}$ from between apo and darunavir-bound PR. See figure 5 for structural element designations and visualization.

| Structural Element | | Relative change (%) | Contribution (%) |
|---|---|---|---|
| Monomer A | Active site | 0.88 | 1.61 |
| | Flap | 10.85 | 18.25 |
| | α-helix | 2.34 | 5.12 |
| | β-sheet 1 | 6.27 | 10.85 |
| | β-sheet 2 | 2.52 | 4.92 |
| Monomer B | Active site | 0.83 | 1.48 |
| | Flap | 3.41 | 6.31 |
| | α-helix | 6.70 | 13.37 |
| | β-sheet 1 | 3.52 | 6.19 |
| | β-sheet 2 | -3.77 | -7.35 |
| Intermolecular | Terminal β-sheet | 3.32 | 5.73 |

## Figure captions.

**Figure 1. Timescales and frequencies of physical events associated with protein molecules**

Collective motions of protein molecules occur as breathing modes (5-15 $cm^{-1}$) and vibrational dynamics (15-50 $cm^{-1}$) in the low-THz frequencies regime at timescales ranging from ~0.5-7 ps.

**Figure 2. The structure of HIV-1 PR in complex with darunavir (DRV) in cartoon representation and the chemical diagram of DRV.**

**Figure 3. Protein powder model used for MD simulations of neutron vibrational spectroscopy experiments**

Conformationally variable snapshots harvested from one μs MD simulations of HIV-1 protease in solution were used to populate a ten-dimer amorphous ensemble. The ensemble was solvated and cooled to experimental conditions for data collection.

**Figure 4. Inelastic Neutron Scattering experiments and MD simulation of HIV-1 protease systems**

a-b) Experimental INS spectra for the boson peak and the low-frequency regime of PR and PR/DRV samples. Data shown as lines with Savitzky-Golay smoothed (5-point, $2^{nd}$ ordered polynomial) and error as shades.

b-c) Calculated INS spectra of boson peaks and low-frequency regime from MD simulations of PR and PR/DRV experimental models. Data plotted as means ± standard error of the mean (SEM) as shades.

e) Change in mean INS signal intensity (PR/DRV-PR) from 1-60 $cm^{-1}$ from MD simulations. Mean ± SEM as shades with Savitzky-Golay smoothed line (5-point, $2^{nd}$ ordered polynomial).

**Figure 5. Vibrational density of states spectra for MD simulations of HIV-1 protease systems**

a) VDOS ($g(\omega)$) in the low-frequency regime for PR and PR/DRV. Mean ± SEM as shades.

b) Change in VDOS ($g(\omega)$) between ligand-bound PR and apo PR (PR/DRV-PR). Mean ± SEM as shades with Savitzky-Golay smoothed line (5-point, $2^{nd}$ ordered polynomial).

**Figure 6. Changes in VDOS mapped to structural elements of HIV-1 Protease**

a) Cartoon of HIV-1 Protease dimer complexed with darunavir with color-coded labels for characteristic structural elements. Inhibitor and active site residues as sticks. b) PR/DRV dimer with each structural element colored by its contribution to overall change in VDOS of the protein as tabulated in Table 1.

**Figure 7. Change in VDOS for secondary structure elements of HIV-1 protease**

Plots of the change in VDOS ($g(\omega)$) from 1-60 $cm^{-1}$ for a) Monomer A Flap, b) Monomer A β-sheet 1, d) Monomer B α-helix, and e) Monomer B β-sheet 2 color-coded to the PR/DRV dimer structure shown in c). Mean ± SEM as shades with Savitzky-Golay smoothed line (5-point, $2^{nd}$ ordered polynomial).

**Figure 8. Vibrational analysis of HIV-1 protease**

a) $Z_{vib}$ from 1-60 $cm^{-1}$ for the PR and PR/DRV systems.

b) Change in VDOS ($g(\omega)$) and change in $Z_{vib}$ between PR/DRV and PR from 1-60 $cm^{-1}$. Lines are shown with Savitzky-Golay smoothing and SEM.

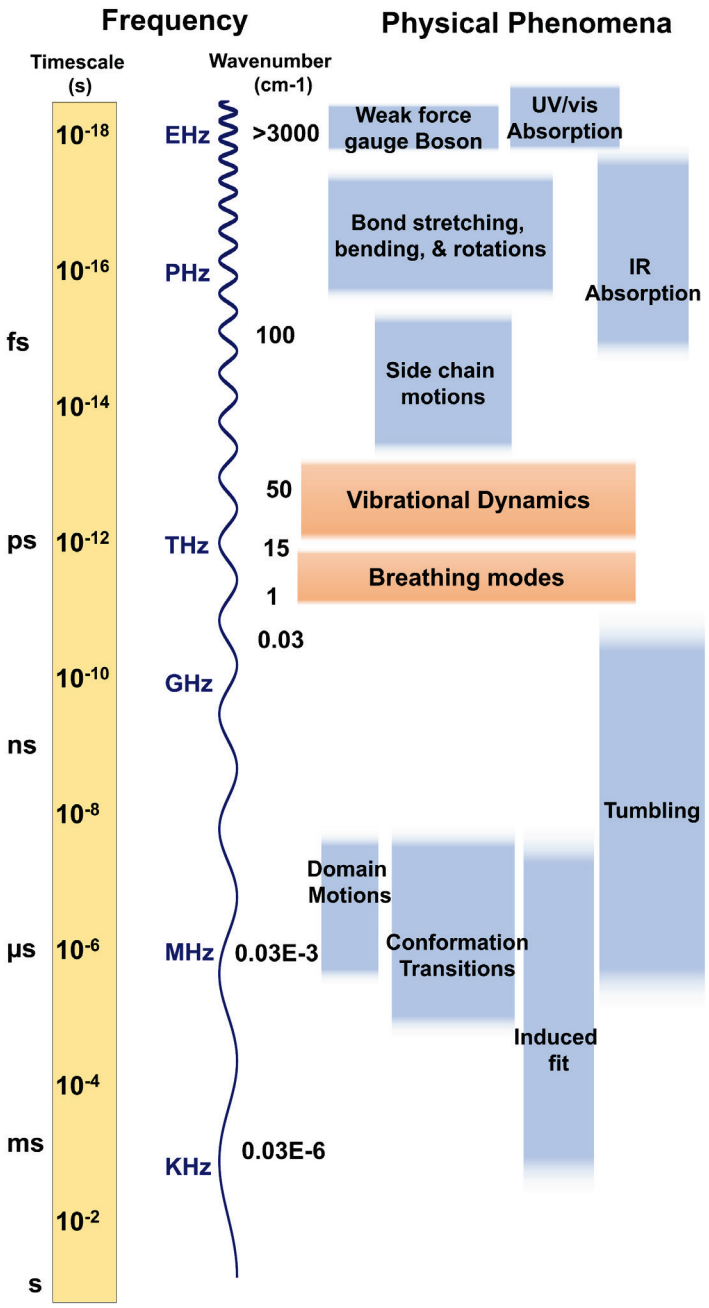
Frequency
Physical Phenomena
Timescale (s)
Wavenumber (cm-1)
10-18
EHz
>3000
Weak force gauge Boson
UV/vis Absorption
Bond stretching, bending, & rotations
IR Absorption
10-16
PHz
fs
100
Side chain motions
10-14
50
Vibrational Dynamics
ps
10-12
THz
15
Breathing modes
1
0.03
10-10
GHz
ns
Tumbling
10-8
Domain Motions
Conformation Transitions
Induced fit
μs
10-6
MHz
0.03E-3
10-4
ms
KHz
0.03E-6
10-2
s

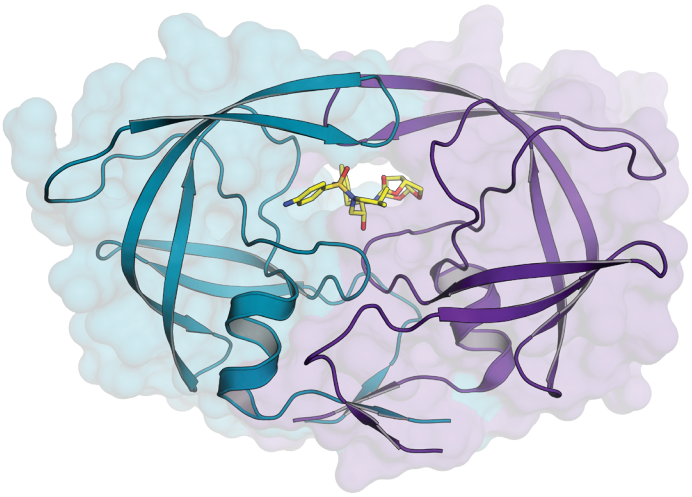

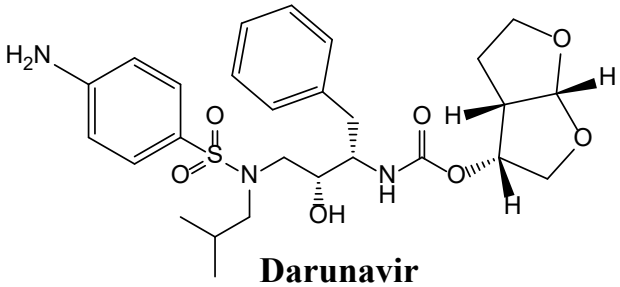


**Darunavir**

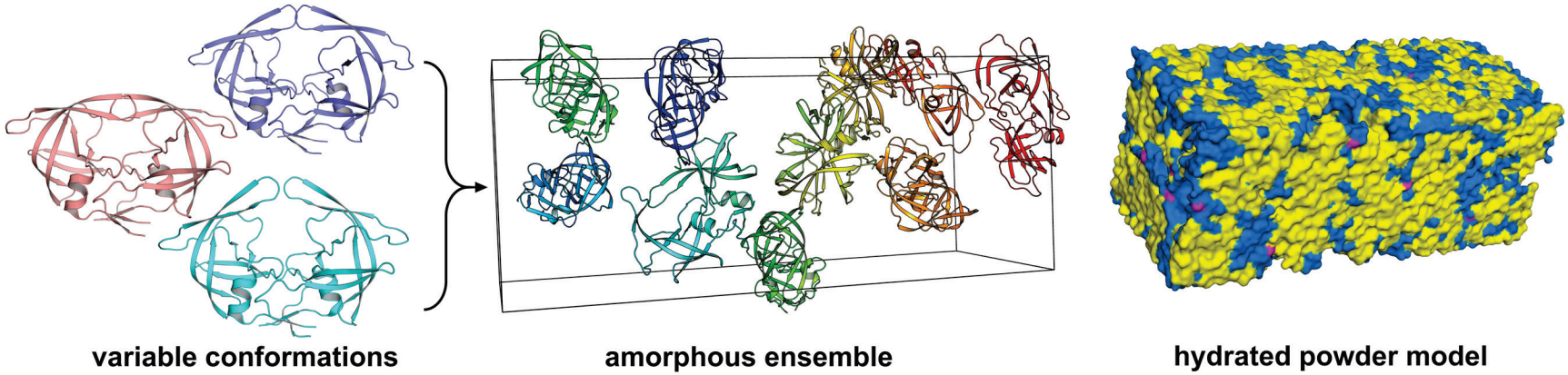
variable conformations
amorphous ensemble
hydrated powder model

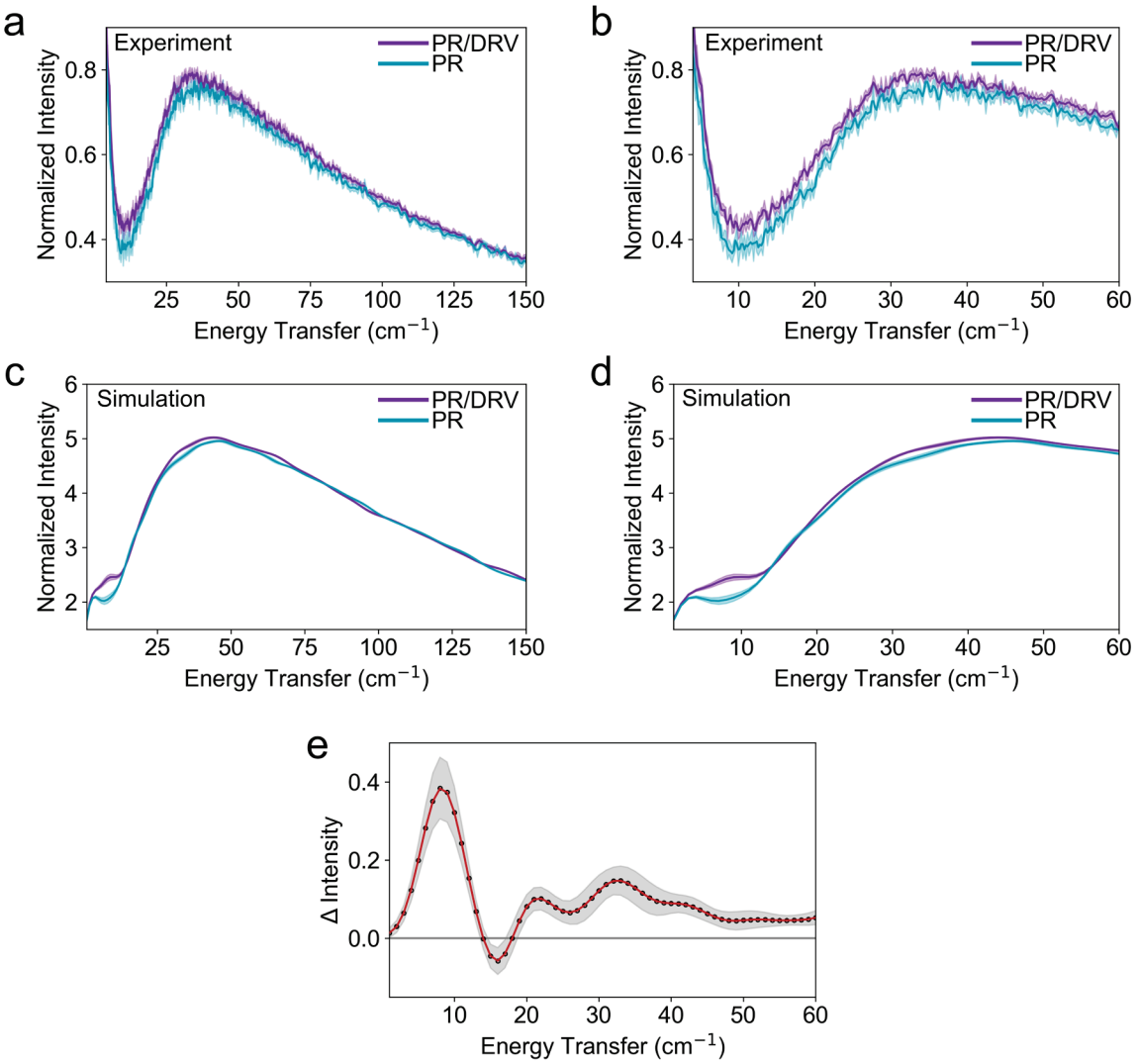
a
Experiment
PR/DRV
PR
Normalized Intensity
0.4
0.6
0.8
25
50
75
100
125
150
Energy Transfer (cm$^{-1}$)
b
Experiment
PR/DRV
PR
Normalized Intensity
0.4
0.6
0.8
10
20
30
40
50
60
Energy Transfer (cm$^{-1}$)
c
Simulation
PR/DRV
PR
Normalized Intensity
2
3
4
5
6
25
50
75
100
125
150
Energy Transfer (cm$^{-1}$)
d
Simulation
PR/DRV
PR
Normalized Intensity
2
3
4
5
6
10
20
30
40
50
60
Energy Transfer (cm$^{-1}$)
e
Δ Intensity
0.0
0.2
0.4
10
20
30
40
50
60
Energy Transfer (cm$^{-1}$)

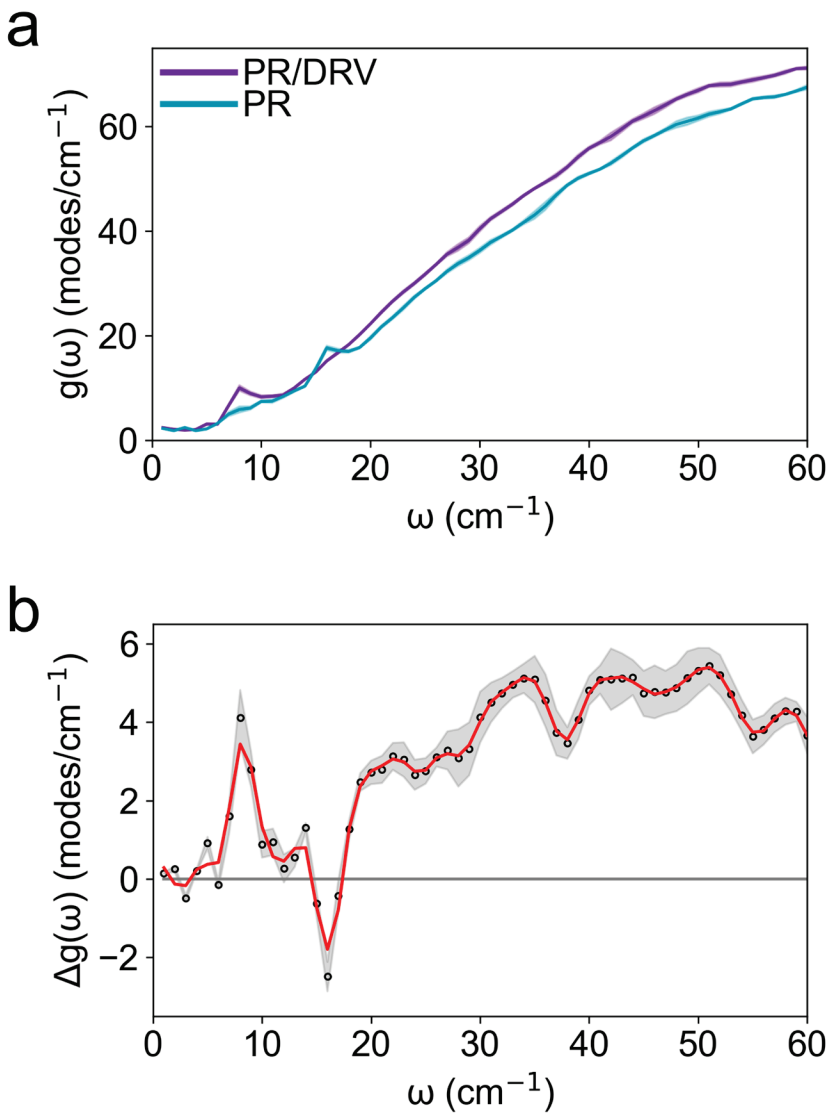
a
PR/DRV
PR
g(ω) (modes/cm$^{-1}$)
ω (cm$^{-1}$)
b
Δg(ω) (modes/cm$^{-1}$)
ω (cm$^{-1}$)

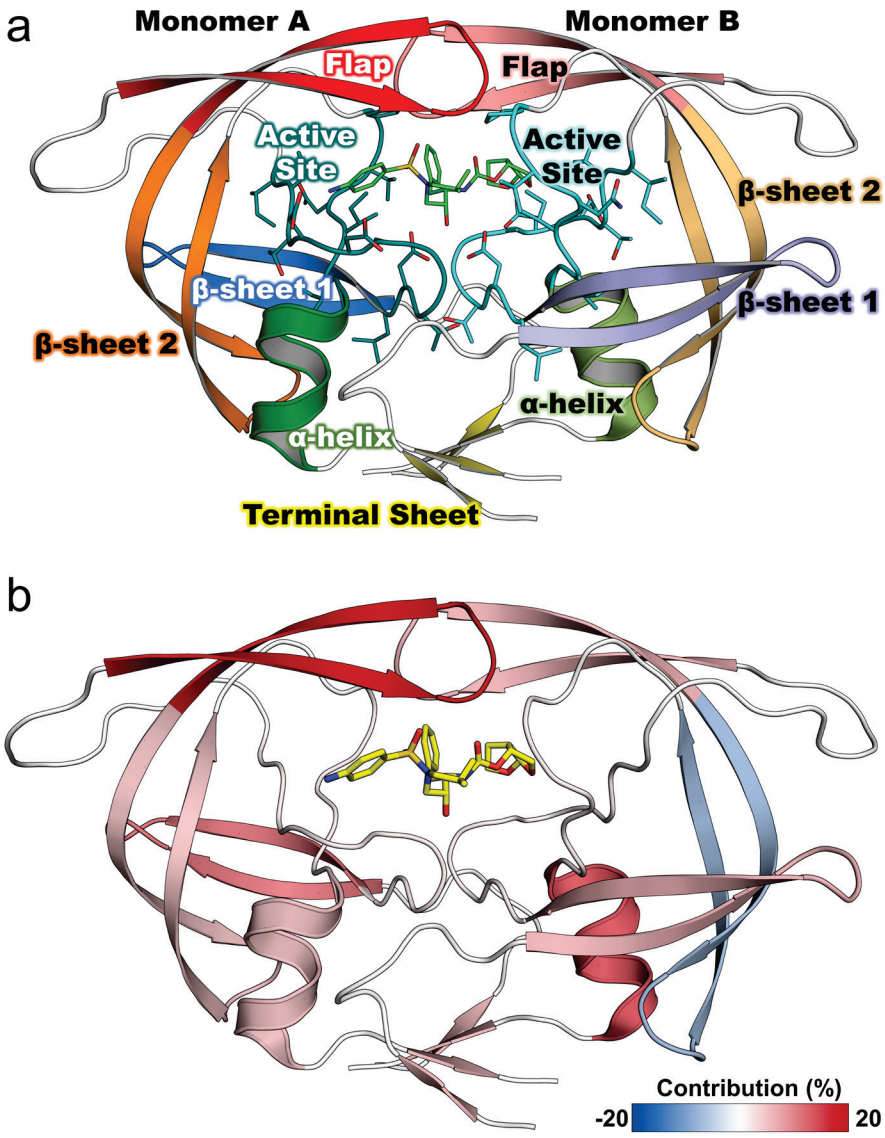
a
Monomer A
Monomer B
Flap
Flap
Active Site
Active Site
β-sheet 2
β-sheet 1
β-sheet 1
β-sheet 2
α-helix
α-helix
Terminal Sheet
b
Contribution (%)
-20
20

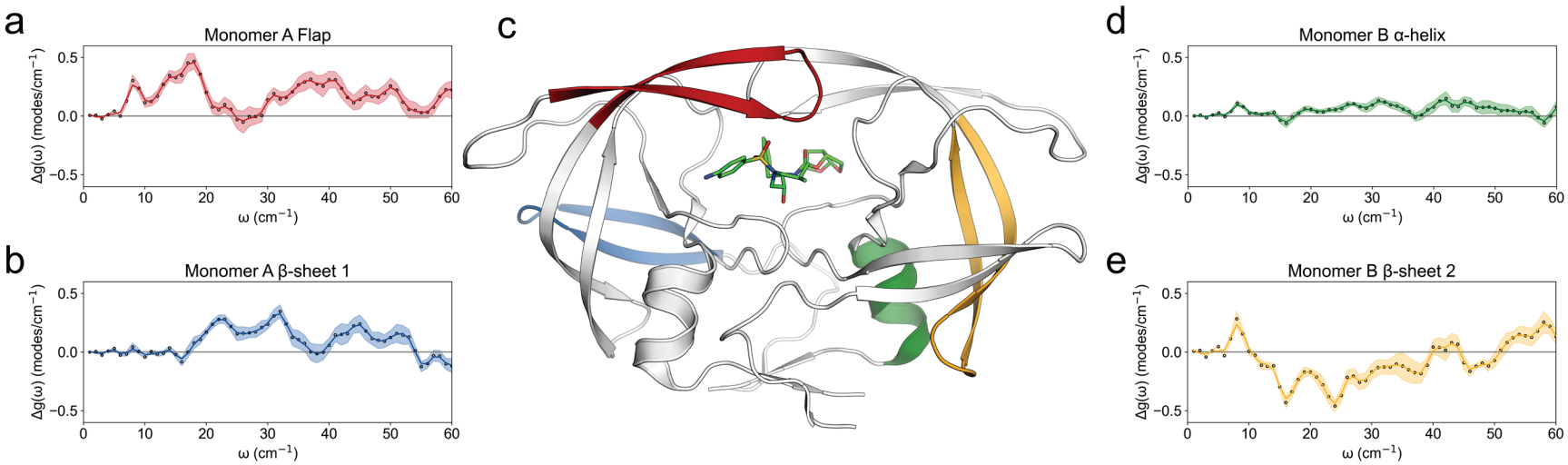
a
Monomer A Flap
b
Monomer A β-sheet 1
c
d
Monomer B α-helix
e
Monomer B β-sheet 2
Δg(ω) (modes/cm⁻¹)
ω (cm⁻¹)
0.5
0.0
−0.5
0
10
20
30
40
50
60

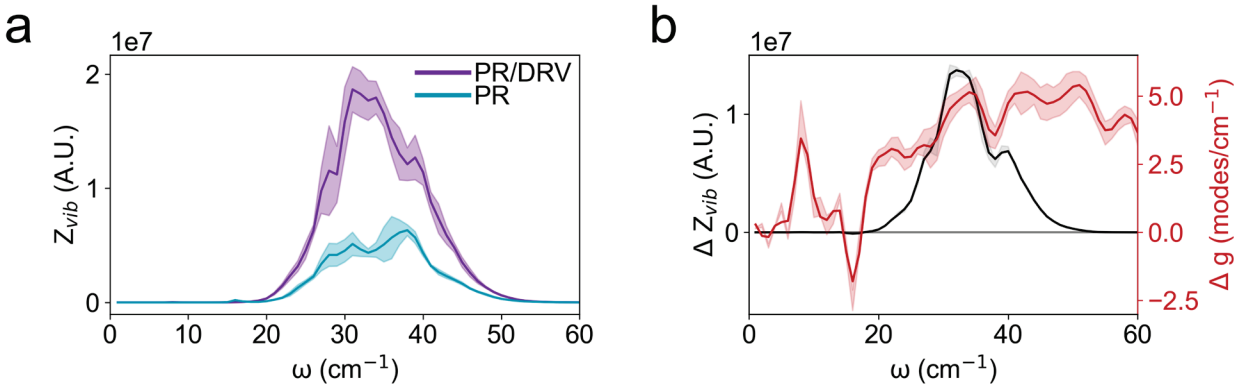
a
1e7
2
1
0
$Z_{vib}$ (A.U.)
PR/DRV
PR
0
10
20
30
40
50
60
ω ($cm^{-1}$)
b
1e7
1
0
Δ $Z_{vib}$ (A.U.)
5.0
2.5
0.0
−2.5
Δ g (modes/$cm^{-1}$)
0
20
40
60
ω ($cm^{-1}$)